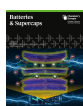




# Electrochemical Activation of 2D MXene-Based Hybrid for High Volumetric Mg-Ion Storage Capacitance



Min Gyu Jung<sup>+</sup>,<sup>[a]</sup> Girish Sambhaji Gund<sup>+</sup>,<sup>[a]</sup> Yury Gogotsi,<sup>\*[b]</sup> and Ho Seok Park<sup>\*[a, c]</sup>

Electrochemical capacitors are considered as a strong candidate of energy storage device due to their high power density and long cycle lifetime. However, commercial carbon-based electrochemical capacitors provide only about  $60 \text{ F cm}^{-3}$  of volumetric capacitance due to low packing density and intrinsic areal capacitance. Two-dimensional (2D) transition metal carbides/nitrides, known as MXenes, have received attention due to their high electronic conductivity, surface modification, and abilities to achieve superior ion intercalation and packing density. Here,

we report the improved volumetric Mg-ion storage capacitance of 2D MXene/reduced graphene oxide (rGO) hybrid through electrochemical activation. Along with high volumetric capacitance of  $439 \text{ F cm}^{-3}$  at  $2 \text{ mV s}^{-1}$ , MXene/rGO hybrid electrode exhibits superior capacitive retention of 87% after 10,000 cycles in aqueous Mg-ion system. Thus, our hybrid electrode and electrochemical activation approach opens new avenues to store Mg and other multivalent ions for high volumetric capacitance of electrochemical capacitors.

## 1. Introduction

Motivated by the fact that consumption of fossil fuel causes serious environmental issues,<sup>[1]</sup> electrical energy storage is critical for achieving sustainable energy future.<sup>[2]</sup> Supercapacitors, known as electrochemical capacitors, have advantages over batteries in terms of their higher power density and longer cycle lifetime than batteries.<sup>[1,3]</sup> Supercapacitors of two types depend on charge storage mechanism at the electrode-electrolyte interface: one stores charges through an electrostatic adsorption at the electrode/electrolyte interface, so-called electric double layer capacitor (EDLC), and second does through a reversible surface redox reaction or fast intercalation/deintercalation, so-called pseudocapacitor.<sup>[4]</sup> The electrode materials are a key component to determine performance metrics of supercapacitors.<sup>[5]</sup> The high volumetric capacitance of electrode material with long cycling lifetime is needed to miniaturize supercapacitors and to use it efficiently as a power source to electronic circuit.<sup>[1,3]</sup> However, commercial carbon-

based EDLCs provide only about  $60 \text{ F cm}^{-3}$  of volumetric capacitance due to low packing density and intrinsic double-layer capacitance.

Two-dimensional (2D) nanomaterials such as graphene, MXene, transition metal chalcogenides, and black phosphorous are strong candidates to replace carbon-based EDLC due to their large accessible area, high redox capacitance, and abundant surface chemistries.<sup>[1,3,4,6–12]</sup> In order to resolve low volumetric capacitance issue, the approach of liquid-mediated dense integration of 2D graphenes has been employed, demonstrating four-fold increase in volumetric capacitance.<sup>[3]</sup> In addition to the modification of electrode materials, multivalent ion carriers such as Mg, Al, and Zn ions have been accommodated to improve the specific capacitance.<sup>[13]</sup> However, the charge storage kinetics became sluggish due to slow diffusion and high activation energy, as well as the charge storage efficiency was lowered due to irreversible reactions.<sup>[4]</sup> The physical, chemical, and electrochemical activation have been undertaken for easy ion accommodation and low charge transfer activation.<sup>[1,3,15–18]</sup>

Here, we report electrochemical activation of  $\text{Ti}_3\text{C}_2\text{T}_x$  (MXene)/reduced graphene oxide (MXrGO) hybrid material through ionic intercalation/deintercalation in aqueous  $1 \text{ M Na}_2\text{SO}_4$  electrolyte for the greatly improved volumetric capacitance. The electrochemically activated MXrGO hybrid electrode (EA-MXrGO) provides  $439 \text{ F cm}^{-3}$  of volumetric capacitance at  $2 \text{ mV s}^{-1}$  within the wide potential window of  $-0.5$  to  $+0.5 \text{ V}$  vs Ag/AgCl retaining 87% of its capacitance after 10,000 cycles at  $10 \text{ A g}^{-1}$ .

## 2. Results and Discussion

MXene used in the current study was prepared by LiF/HCl etching method and exfoliated to make colloidal solution as reported previously.<sup>[19]</sup> The graphene oxide (GO) colloidal solution was employed to synthesize hybrid material. The

[a] M. Gyu Jung,<sup>+</sup> Dr. G. Sambhaji Gund,<sup>+</sup> Prof. H. Seok Park  
School of Chemical Engineering,  
Sungkyunkwan University,  
2066, Seoburo, Jangan-gu, Suwon 440-746, Korea  
E-mail: phs0727@sksku.edu

[b] Prof. Y. Gogotsi  
A. J. Drexel Nanomaterials Institute and Department of Materials Science and Engineering,  
Drexel University,  
Philadelphia, PA 19104, USA  
E-mail: gogotsi@drexel.edu

[c] Prof. H. Seok Park  
Department of Health Sciences and Technology,  
Samsung Advanced Institute for Health Sciences and Technology (SAIHST),  
Sungkyunkwan University,  
2066, Seoburo, Jangan-gu, Suwon 440-746, Korea

<sup>+</sup> These authors contributed equally to this work.

 Supporting information for this article is available on the WWW under <https://doi.org/10.1002/batt.201900185>

 This publication is part of a joint Special Issue with ChemSusChem focusing on "2D Energy Storage Materials"

MXene, GO, and MXrGO hybrids at the weight ratios of MXene to GO of 1:1, 2:1, and 3:1 were freeze dried and subjected to two-step annealing treatment (250 °C - 1 hr and 600 °C - 1 hr) for thermal reduction into rGO in inert Ar atmosphere, as schematically illustrated in Figure 1. The as-prepared materials were denoted as MXene, rGO, MXrGO11, MXrGO21, and MXrGO31, respectively. Furthermore, the resulting electrodes based on these materials were electrochemically activated in Na<sub>2</sub>SO<sub>4</sub> aqueous electrolyte and denoted as EA-MXene, EA-rGO, EA-MXrGO11, EA-MXrGO21, and EA-MXrGO31, respectively.

Figure 2 shows field emission scanning electron microscope (FE-SEM) images of MXene and MXrGO hybrid powdery samples. All images clearly demonstrated flake-like morphologies corresponding to 2D structure of both MXene and rGO (see Figure S1). Additionally, a few MXene particles revealed exfoliated accordion structure as shown Figure 2a and b. But, the processes followed during hybrid synthesis led to well exfoliated MXene flakes strongly adhered the rGO sheets without any aggregation, as illustrated in Figure 2c-h. Apart

from this, the magnified images in Figure 2b, d, f, and h revealed few-layer structure of MXene flakes. Thus, the anchoring of MXene on rGO sheets stabilizes MXrGO hybrid physically, but still allows utilization of deep adsorption sites to store Mg ions.<sup>[4]</sup>

The microstructure and structural analysis of prepared rGO, MXene, and MXrGO11 2D sheets were analyzed by transmission electron microscopy (TEM), high resolution-TEM (HR-TEM), selective area electron diffraction (SAED), and scanning TEM-energy dispersive X-ray spectroscopy (STEM-EDS) elemental mapping, as shown in Figure 3a-h. The few-layered, stacked, and 2D sheet-like features of rGO, MXene, and MXrGO11 hybrids are clearly observed in Figure 3a-c. The existence of rGO and MXene sheets in MXrGO hybrid as clearly demonstrated by red arrow and white arrow marks, respectively in Figure 3c. The SAED patterns of rGO, MXene, and MXrGO hybrid demonstrated hexagonal symmetry (Figure 3d-f) of the atomic arrangement in the [001] orientation of the planes of few layered 2D sheet.<sup>[20]</sup> The additional diffraction spots

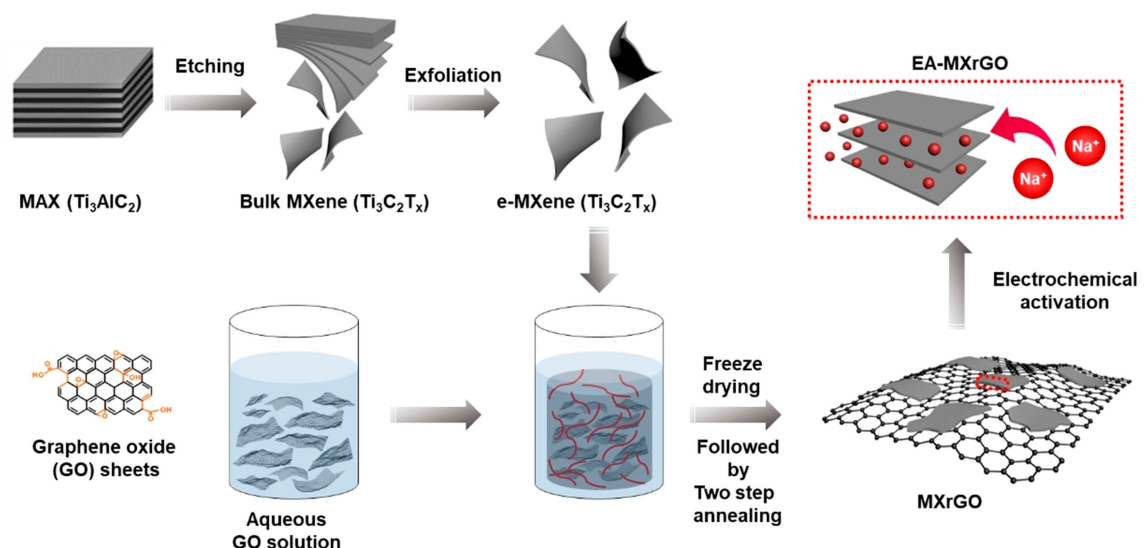


**Figure 1.** Schematic representation of preparation of MXrGO hybrid materials and electrochemical activation of electrodes based on hybrid materials in 1 M Na<sub>2</sub>SO<sub>4</sub> aqueous electrolyte.

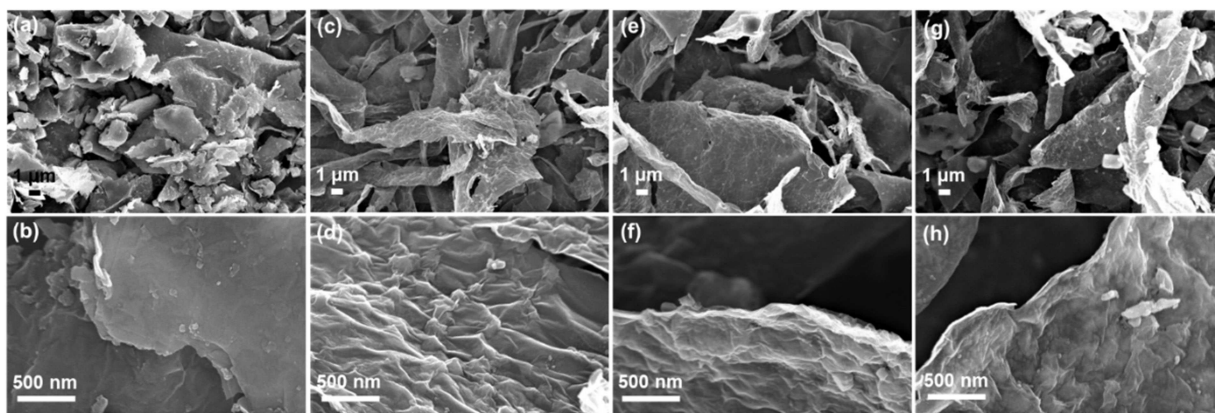


**Figure 2.** FE-SEM images of (a, b) MXene, (c, d) MXrGO11, (e, f) MXrGO21, and (g, h) MXrGO31 powder samples.

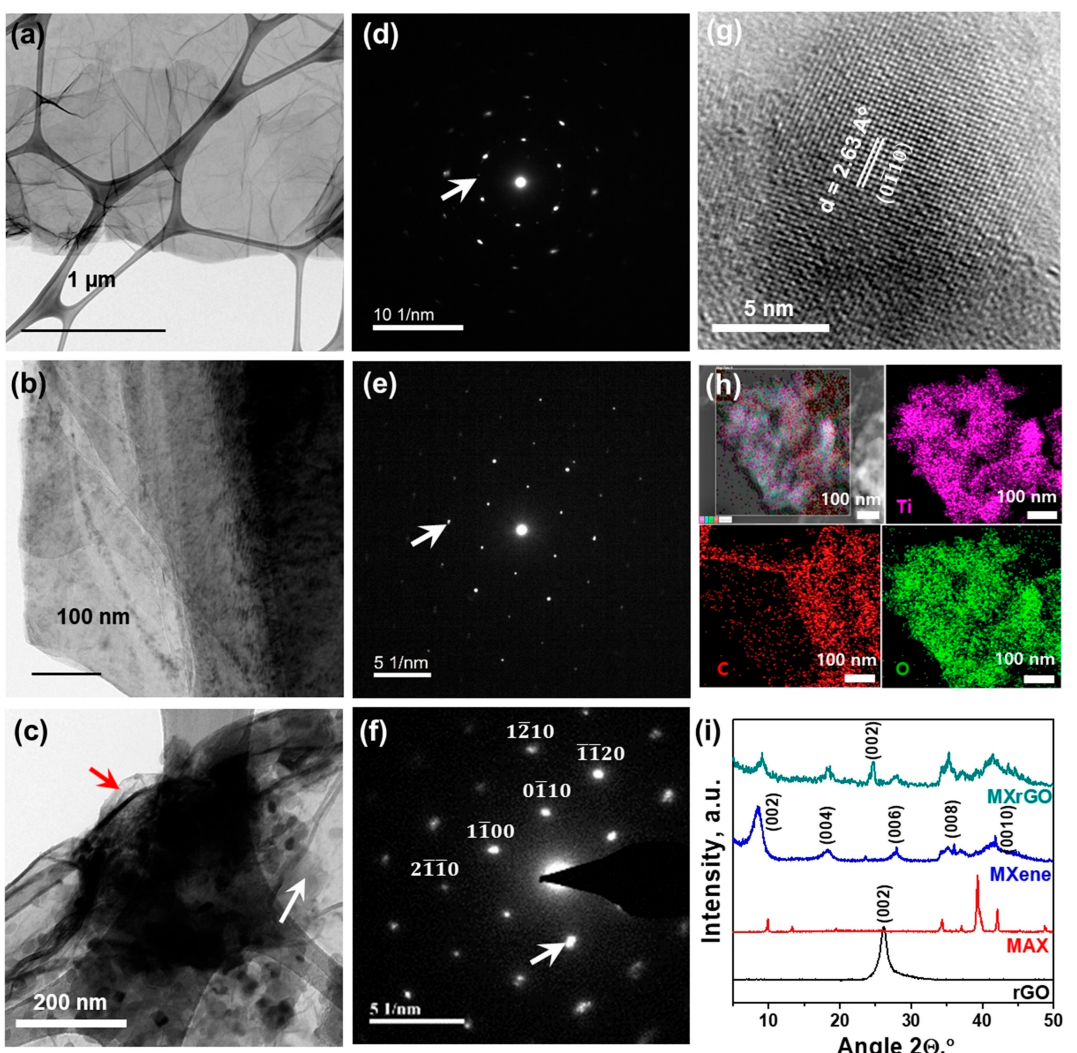


**Figure 3.** TEM images (a–c) and SAED patterns (d–f) of rGO (a, d), MXene (b, e), and MXrGO11 (c, f) sheets. HR-TEM image (g) and STEM-EDS elemental mapping (h) of MXrGO11. (i) XRD patterns of rGO, MAX, MXene, and MXrGO11 powder samples.

(marked by white arrows) in SAED patterns generated from the superimpositions of the few layers<sup>[21–23]</sup> are consistent with the observations from SEM and TEM images. HR-TEM image of MXrGO11 hybrid sheet demonstrated lattice fringes with interlayer spacing of 2.63 Å corresponding to a hexagonal structure of MXene, as illustrated in Figure 3g. Apart from this, STEM-EDS mapping indicates chemical purity of MXrGO hybrid containing Ti, C, O, and F elements without any other impurities (Figure 3h).

X-ray diffraction (XRD) patterns of rGO,  $Ti_3AlC_2$  (MAX), MXene, and MXrGO11 hybrid powder samples are displayed in Figure 3i. The diffraction peaks at 9.5°, 39°, and 41.8° were observed for the MAX powder sample, assigned to the (002), (104), and (105) planes of MAX phase.<sup>[22]</sup> The broadening of diffraction peaks for MXene sample confirmed crystallinity decrement of MAX sample after LiF/HCl etching.<sup>[24]</sup> MXene and MXrGO patterns revealed peaks for [001] oriented hexagonal symmetric planes of MXene.<sup>[11]</sup> Additionally, the characteristic diffraction peaks of MAX and rGO assigned to (002) plane

observed at 2θ angles of 9.9 and 26.2° were shifted towards lower angles of 8.6 and 24.7° due to increased interlayer spacing of 6.8 and 5.9 nm due to etching of Aluminum layers with the substitution by surface terminal groups in MXene and MXene sheets sandwiched between rGO sheets in the MXrGO11 hybrid, respectively.<sup>[22]</sup> Thus, the successful etching, exfoliation, and hybridization of 2D materials were confirmed.<sup>[24]</sup>

The electrochemical properties of all prepared electrodes, rGO, MXene, and MXrGO hybrids, were measured in 1 M  $MgSO_4$  aqueous electrolyte solution using three-electrode configured electrochemical cell, as illustrated in Figure 4. Being neutral and inexpensive, Mg-salt based electrolyte is environmentally and chemically safe for energy storage technology.<sup>[11]</sup> The cyclic voltammetric (CV) curves of pristine materials and hybrids with different compositions are shown in Figures 4a, b (scan rate of 10 mV s<sup>-1</sup>). The irreversible oxidative reaction peak under anodic potential (>0.4 V vs Ag/AgCl) was observed for pristine MXene, absent for rGO, and suppressed for MXrGO11 electro-

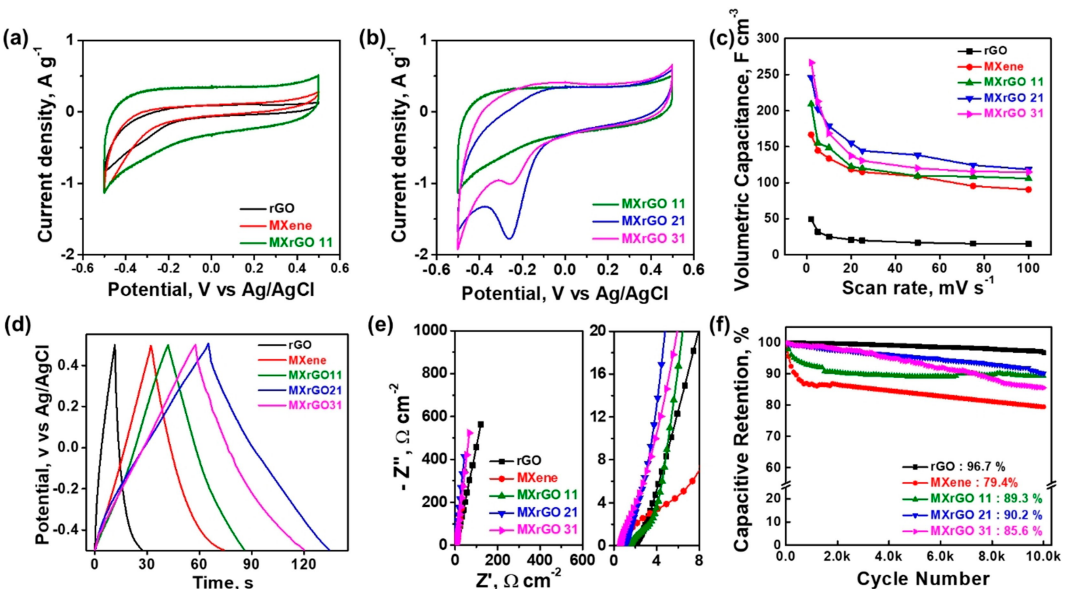


**Figure 4.** CV curves of (a) pristine MXene, rGO electrodes and MXrGO11 hybrid electrode, and (b) different MXrGO hybrid electrodes at constant scan rate of 10 mV s<sup>-1</sup>. (c) Rate performance, (d) GCD curves at 2 A g<sup>-1</sup> current density, (e) Nyquist plots, and (f) Cycling stability for 10,000 cycles at 10 A g<sup>-1</sup> current density of pristine (rGO, MXene) and hybrid (MXrGO11, MXrGO21, MXrGO31) electrodes.

des. Because rGO electrodes store charges primarily through physical EDLC mechanism, in contrast to pseudocapacitive mechanism of MXene electrodes, pristine MXene can be consumed. Whereas, effective MXene anchoring on rGO sheets and hybrid charge storage mechanism may help to suppress irreversible reactions and promote reversible pseudocapacitive charge storage of MXrGO hybrid electrodes. On the other side, sluggish intercalation/de-intercalation peak in the negative potential window ( $< -0.2$  V vs Ag/AgCl) was observed for pristine rGO and MXene electrodes and diminished for MXrGO11 hybrid electrode. Few-layer structure of pristine 2D rGO and MXene contains minute shallow adsorption sites and limits fast intercalation/de-intercalation and utilization of deep adsorption sites. Contrary, the MXrGO11 hybrid can offer improved shallow adsorption sites with expanded deep adsorption sites, which may be due to the 2D hybrid architecture confirmed by increased interplanar distance for (002) plane of rGO in XRD examination. Thus, the hybrid MXrGO11 architecture improves material utilization and thus Mg<sup>2+</sup> ion storage.

The comparison of CV curves of MXrGO hybrid electrodes with increasing MXene content at constant 10 mV s<sup>-1</sup> of scan rate, illustrated in Figure 4b, reveals little change in irreversible oxidative reaction peak, but significant elevation of sluggish intercalation/de-intercalation peaks below  $-0.4$  V. Whereas, MXrGO21 demonstrated an increased surface redox peak around  $-0.24$  V, related to Mg-ion intercalation, compared to MXrGO11 and MXrGO31. This is because of the anchoring effect by rGO and inhibited restacking chemistry for hybrid materials is diminished with increasing MXene content, while the optimized composition MXrGO21 produces synergistic results of both phenomena. Thus, the optimized MXrGO21 hybrid

electrodes can store a large number of ions per unit of volume owing to increased accessibility of active material.

The CV curves and estimated volumetric capacitance from each curve with varying scan rate for pristine and hybrid electroactive materials are displayed in Figure S2a-e and Figure 4c. The CV curves at different scan rates had similar shapes to the ones recorded at 10 mV s<sup>-1</sup> scan rate. The volumetric capacitance of rGO, MXene, MXrGO11, MXrGO21, and MXrGO31 electrodes were diminished from-to (49–15, 167–90, 209–106, 246–119, and 267–115 F cm<sup>-3</sup>, respectively.) with increasing scan rate (2–100 mV s<sup>-1</sup>). This capacitance decrement with increasing scan rate leads to capacitive retention of 30.6, 53.9, 52.1, 48.4, and 43.1 %, respectively. The volumetric capacitance of MXrGO31 is a little higher but stacking decreases the rate capability with increasing MXene content. Thus, the MXrGO21 hybrid electrode showed the optimum capacitance towards Mg<sup>2+</sup> ion storage per unit of volume of active materials with optimum rate capability.

Furthermore, galvanostatic charge-discharge (GCD) curves for pristine and hybrid materials were measured within the potential window of  $-0.5$  to  $+0.5$  V vs Ag/AgCl at constant current density of 2 A g<sup>-1</sup>, as illustrated in Figure 4d. The GCD profiles of pristine rGO and MXene electrodes revealed plateaus below  $-0.4$  V potential, which may originate from a sluggish intercalation/de-intercalation of Mg<sup>2+</sup> ions or irreversible redox reaction. This feature in GCD curves disappeared for MXrGO11 and MXrGO21-based electrodes, but again appeared for MXrGO31 (Figure 4d). Additionally, the calculated volumetric capacitance for all materials as a function of current density from GCD measurements also demonstrated relatively high volumetric capacitance for MXrGO21 with optimum rate capability (see Figure S2f). The estimated charge transfer and energy conservation efficiencies, so called coulombic and

energy efficiencies, respectively, as a function of current density from GCD measurements are illustrated in Figure S3. There is not much difference in coulombic efficiency, but synergy of hybridization allows fast charge kinetics even at high current density. Thus, the GCD measurements agree with the CV measurements and hence support the charge kinetics control within the 2D hybrid material through restacking inhibition.

In order to provide additional information about charge dynamics in the pristine and hybrid electrodes, we carried out electrochemical impedance spectroscopy (EIS) measurements in the frequency range of 100 mHz to 100 kHz, as demonstrated in Figure 4e. Nyquist plots exhibit semicircles in the high frequency region (see the zoomed plot) followed by a straight line in the low frequency region. The intercept of semicircle on the real impedance axis, diameter of semicircle, and slope of the vertical line correspond to equivalent series resistance, charge transfer resistance, and diffusion of ions (or material accessibility to ions) within electrode material, respectively. From Figure 4e, the pristine rGO and MXene electrodes were observed owing domination of slower ion diffusion and larger charge transfer resistance compared to hybrid electrodes. The equivalent series resistance and charge transfer resistance of hybrid materials decreased with increasing MXene content, while material accessibility to ions in the low frequency region improved up to the optimum composition and then decreased. Thus, the charge dynamics was enhanced with the hybrid 2D materials (MXrGO11 and MXrGO21), but became sluggish with increasing content of MXene (MXrGO31) and well matched with the conclusions from CV and GCD measurements.

To confirm anchoring of MXene sheets on rGO sheets, we performed comparative long cycling stability studies of all electrodes through GCD measurements for 10,000 cycles at constant current density of  $10 \text{ A g}^{-1}$ , as shown in Figure 4f. The highest capacitance retention of 96.7% was observed for rGO electrodes owing to their physical EDLC charge storage mechanism. Contrary, pristine MXene electrode degraded rapidly until initial 1,000 cycles (up to 86.7%), then with constant rate, and showed the relative capacitive retention of 79.4% after 10,000 cycles. Whereas, relatively high capacitance retention was observed for all hybrid MXrGO electrodes compared to pristine MXene electrode. Specifically, MXrGO11 electrode lost about ~7.5% of capacitance for initial 1,000 cycles and further only ~3.2% for the next 9,000 cycles. While, MXrGO21 and MXrGO31 hybrid electrodes showed capacitance loss with the constant rate, which increased with MXene content. Thus, the MXrGO21 hybrid material with the optimum composition revealed the best stabilization of MXene on rGO sheets.

To further enhance the material utilization and improve access to deep adsorption sites in the optimum MXrGO21 electrode (further noted as MXrGO), we performed electrochemical activation of this electrode for 300 CV cycles in 1 M  $\text{Na}_2\text{SO}_4$  at  $20 \text{ mV s}^{-1}$  of scan rate in same potential window of  $-0.5$  to  $+0.5 \text{ V vs Ag/AgCl}$ , as illustrated in Figure 5a.  $\text{Na}^+$  ions were selected because they could expand the stacked layered structure of MXrGO during CV cycling, as seen in Figure 5a. Thus, opening the deep adsorption sites for easy intercalation/de-intercalation of Mg ions. This electrochemically activated hybrid electrode was labeled as, EA-MXrGO, and dipped directly

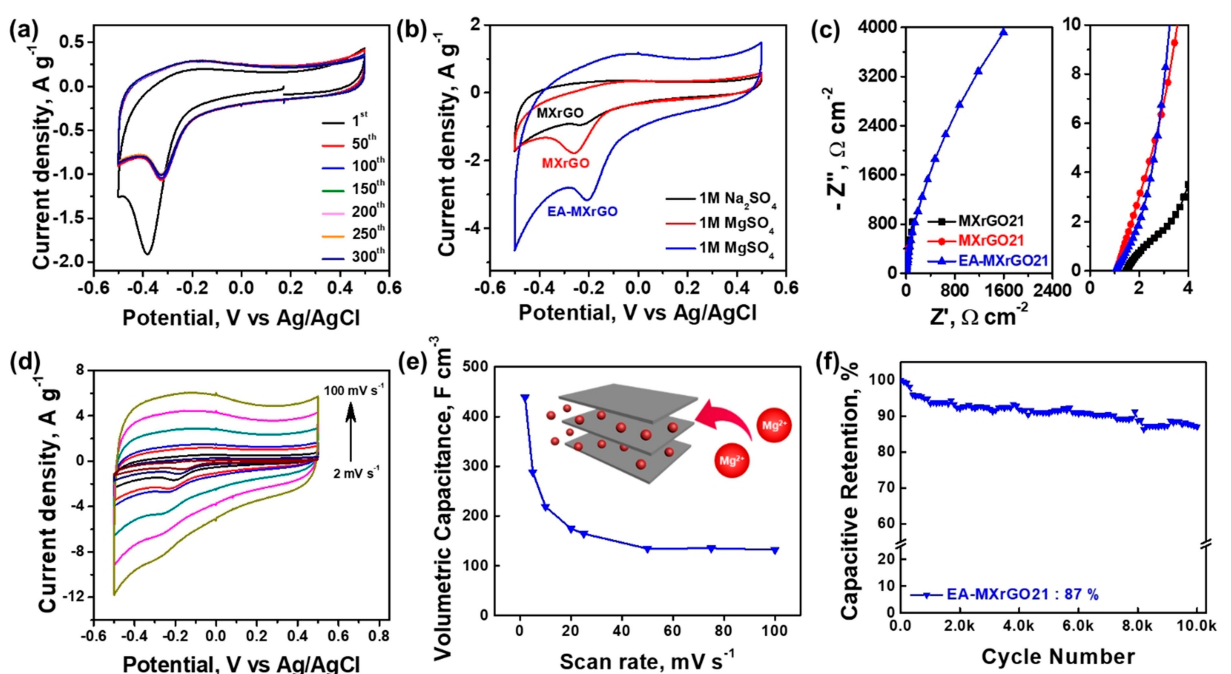


**Figure 5.** (a) Different cycles of CV curve for electrochemical activation of hybrid MXrGO electrode in 1 M  $\text{Na}_2\text{SO}_4$  electrolyte at  $20 \text{ mV s}^{-1}$  of scan rate. Comparative (b) CV curves and (c) Nyquist plots of MXrGO in 1 M  $\text{Na}_2\text{SO}_4$  electrolyte with MXrGO and EA-MXrGO electrodes in 1 M  $\text{MgSO}_4$  electrolyte at  $10 \text{ mV s}^{-1}$  of scan rate. (d) CV curves at changing scan rate, (e) Rate performance, and (f) Cycling stability for 10,000 cycles at constant current density of  $10 \text{ A g}^{-1}$  of EA-MXrGO hybrid electrode.

in 1 M  $\text{MgSO}_4$  electrolyte for further electrochemical measurements. The comparative CV curves and Nyquist plots of MXrGO electrode in 1 M  $\text{Na}_2\text{SO}_4$  electrolyte with MXrGO and EA-MXrGO electrodes in 1 M  $\text{MgSO}_4$  electrolyte at the scan rate of 10  $\text{mVs}^{-1}$  are displayed in Figure 5b. The two-fold increment of current density for EA-MXrGO electrode was observed compared to MXrGO. Additionally, imaginary impedance in the Nyquist plot is a direct measure of capacitive behavior, which has been increased considerably for EA-MXrGO electrode (Figure 5c). Additionally, the enhancement of charge dynamics was detected in the zoomed high frequency region of the Nyquist plot. Apart from this,  $\text{Na}^+$  ions are larger and lighter than  $\text{Mg}^{2+}$  ions. This facilitates a reversible intercalation/deintercalation of  $\text{Na}^+$  ions and effective slow activation to open deep adsorption sites, as confirmed by observed good coulombic efficiency of MXrGO electrode in 1 M  $\text{Na}_2\text{SO}_4$  electrolyte and EA-MXrGO electrode in 1 M  $\text{MgSO}_4$  electrolyte.

The pseudo-rectangular shape of CV curves at varying scan rates (2–100  $\text{mVs}^{-1}$ ) for EA-MXrGO corresponds to the fast intercalation/de-intercalation (pseudocapacitive) charge storage mechanism, as shown in Figure 5d. The calculated volumetric capacitance of EA-MXrGO electrode from CV curves at varying scan rate was illustrated in Figure 5e. The maximum capacitance per unit volume of EA-MXrGO of about  $\sim 439 \text{ Fcm}^{-3}$  was achieved at 2  $\text{mVs}^{-1}$  scan rate and decreased with increasing scan rate down to  $132 \text{ Fcm}^{-3}$  at 100  $\text{mVs}^{-1}$ . Thus, the large increase of capacitance per unit volume ( $193 \text{ Fcm}^{-3}$ ) of material at low scan rate was achieved, compared to only  $13 \text{ Fcm}^{-3}$  at high scan rate. Although the hybrid 2D material was electrochemically activated to open the deep adsorption sites (as illustrated in inset of Figure 5e), its laminar structure still limits fast intercalation/de-intercalation of ions at high scan rate, possibly due to mass and charge of  $\text{Mg}^{2+}$  ions and insufficient volume expansion of the layered structure. This volumetric capacitance of MXene based hybrid material for Mg ion storage is comparable to the values reported in previous studies (see Table S1).<sup>[1,25–27]</sup>

Furthermore, the cycling stability of EA-MXrGO hybrid electrode was also studied for 10,000 GCD cycles at 10  $\text{A g}^{-1}$  current density. The change of capacitive retention with cycle number is shown in Figure 5f, which also exhibited capacitance loss with constant rate, similar to the MXrGO21 hybrid electrode. The observed capacitance retention for EA-MXrGO electrode is 87% after 10,000 cycles. This shows that the electrochemical activation did not significantly improve the cycling stability. Additionally, the comparative electrochemical study of electrochemically activated pristine materials (EA-rGO and EA-MXene) and hybrid (EA-MXrGO11, EA-MXrGO21, EA-MXrGO31) electrodes was also performed (see Figure S4). The comparative examination of performance after electrochemical activation is consistence in terms of high capacitance per unit volume and fast charge dynamics for EA-MXrGO21 at low scan rate. Limited access to deep adsorption sites at high scan rates was observed for all materials. The proposed approach leads to enhancement of material accessibility and increase in their capacitance per unit volume of 2D material through hybridization and electrochemical activation.

### 3. Conclusions

In summary, we have prepared 2D electrochemically activated MXene/rGO hybrid electrode materials of different compositions for capacitive energy storage in  $\text{MgSO}_4$  aqueous electrolyte. The lowest content of 2D MXene in the hybrid facilitated access of Mg ions to shallow and deep adsorption sites by decreasing restacking. The optimum hybrid composition of 2D materials improved capacitance per unit of volume ( $246 \text{ Fcm}^{-3}$ ), optimized rate capability (46.2%), and led to good capacitance retention (90.2%) after 10,000 of charge-discharge cycles as a results of strong interaction of MXene with rGO. Additionally, the electrochemical activation of the hybrid material in 1 M  $\text{Na}_2\text{SO}_4$  electrolyte expanded deep adsorption sites to store Mg ions at low rate. Thus, our work opens the opportunity for further development of 2D hybrid materials capable to store multivalent ions.

## Experimental Section

### Materials

$\text{Ti}_3\text{AlC}_2$  (MAX) Phase powder was purchased from Carbon-Ukraine. Hydrochloric acid (~ 37 wt%, HCl) and Lithium fluoride powder (99.99%, LiF) were bought from Wako Chemicals and Alfa Aesar, respectively, and used as received. Graphene oxide solution of 2 wt % was bought from Angstrom materials Corporation, USA. All other chemicals were of analytical grade, purchased from Sigma-Aldrich and deionized water (DIW) was used as solvent.

### Synthesis of MXene and MXrGO hybrid

MXene ( $\text{Ti}_3\text{C}_2\text{T}_x$ ) was prepared through chemical etching of Al layer from the MAX phase in a mixed solution of 9 M HCl and 7.5 M LiF at 35 °C for 24 hr, as reported elsewhere.<sup>[19]</sup> The collected slurry was washed with DIW through centrifugation at 4500 rpm for 5 min until pH become neutral (about 10 times). Further, the washed slurry was mixed with DIW and suspended to purge  $\text{N}_2$  gas for 2 hr, followed by sonication for full exfoliation. Finally, the solution was centrifuged at 3000 rpm for 10 min and colloidal suspension was separated. Purchased GO solution (2 wt%) was washed through centrifugation at 5000 rpm for 10 min. Then, the MXene and GO colloidal solutions were mixed through stirring (1 hr) followed by tip sonication (1 hr) for producing a homogeneous mixture. The mixed (as hybrid materials) and pristine (reference bare materials) colloidal solutions were freeze dried for 72 hr. Furthermore, freeze dried powders were annealed in two steps, initially at 250 °C for 1 hr and secondly at 600 °C for 1 hr to reduce GO under Ar at 10 °C per min ramping rate of temperature. To vary the composition of hybrid materials, solutions were mixed in 1:1, 2:1, and 3:1 weight ratios of MXene:GO.

### Characterization

The surface morphological features of pristine and hybrid materials were studied by field emission-scanning electron microscope (FE-SEM, LEO SUPRA 55, 10 kV). Whereas, transmission electron microscopy (TEM), selected area electron diffraction (SAED), TEM energy-dispersive X-ray (TEM-EDX) image mapping and spectral analysis were performed to analyse 2D sheet structure using Titan G2 60–300 (FEI, USA) at 120 kV. X-ray photoelectron spectroscopy (XPS,

AXIS Ultra DLD) was performed to probe surface chemical composition of materials using a monochromatic Al-K $\alpha$  (1486.6 eV) with Ag 3d<sub>5/2</sub> energy resolution. X-ray diffraction patterns were measured by a D8 Advance (3 kW) with a  $\Theta/\Theta$  goniometer equipped with a Cu K $\alpha$  radiation generator ( $\lambda=1.54\text{ \AA}$ ). The electrochemical studies like galvanostatic charge-discharge (GCD), cyclic voltammetry (CVs), and electrochemical impedance spectroscopy (EIS) were performed by a Bio-Logic science instrument VSP.

### Electrochemical measurements

The electrochemical measurements were performed in three-electrode cell set-up with a cylindrical platinum rod as a counter-electrode, and saturated Ag/AgCl electrode as reference electrode with 1 M Na<sub>2</sub>SO<sub>4</sub> and 1 M MgSO<sub>4</sub> electrolytes. The slurry of electroactive materials (MXene, rGO, and MXrGO) were composed by 80:10:10 wt% of active material:carbon black powder:polyvinylidene fluoride (PVDF) in N-methyl-2-pyrrolidone (NMP) as a solvent. Furthermore, prepared slurry was coated on pre-cleaned Ti foil as current collector, dried at 80 °C in oven, and used as working electrodes. EIS measurements were carried out in a frequency range from 100 mHz to 100 kHz.

The volumetric capacitance (C<sub>v</sub>) values from CV and GCD curves were calculated through Equations (1) and (2), respectively:<sup>[1]</sup>

$$C_v = \frac{\rho}{m \times v \times \Delta V} \int_{V_c}^{V_o} I(V) dV \quad (1)$$

$$C_v = \frac{2\rho \times I_d \times \int V dt}{m \times (\Delta V)^2} \quad (2)$$

where C<sub>v</sub> is volumetric capacitance (F cm<sup>-3</sup>),  $\int i(V)dV$  is the total average voltammetric charge obtained by integration of positive and negative sweep in CV curve,  $\Delta V$  is the potential window (V), I<sub>d</sub> is the constant discharge current density (A g<sup>-1</sup>),  $\int Vdt$  is the area under discharge curve, m is the mass of the active material on electrode per unit area (1 × 1 cm<sup>2</sup>) dipped in electrolyte, which is estimated through the following relation [Eq. (3)]:

$$m = m_2 - m_1 \quad (3)$$

where m<sub>2</sub> and m<sub>1</sub> are masses of the unit area electrode after and before material coating, respectively. The mass loadings of rGO, MXene, MXrGO11, MXrGO21, and MXrGO31 active materials on electrode are 0.70, 3.52, 1.66, 2.02, and 2.46 mg cm<sup>-2</sup>, respectively. ρ is the density of the electrode calculated using Equation (4):

$$\rho = \frac{m}{t \times A} \quad (4)$$

where A is area of used electrode, we used 1 × 1 cm<sup>2</sup>, and t is the average thickness of electrode calculated by Equation (5):

$$t = t_2 - t_1 \quad (5)$$

where t<sub>2</sub> and t<sub>1</sub> are average thicknesses of the unit area of electrode after and before material coating, respectively measured by digital micrometer screw gauge at different positions.

### Acknowledgments

This work was supported by the National Research Foundation of Korea (NRF) grant funded by the Korea government (MSIT) (NRF-2018R1C1B6008599).

**Keywords:** 2D materials • MXene • Mg ion • volumetric capacity • supercapacitors

- [1] M. R. Lukatskaya, O. Mashtalir, C. E. Ren, Y. Dall'Agnese, P. Rozier, P. L. Taberna, M. Naguib, P. Simon, M. W. Barsoum, Y. Gogotsi, *Science* **2013**, 341, 1502–1505.
- [2] M. Y. Suberu, M. W. Mustafa, N. Bashir, *Renewable Sustainable Energy Rev.* **2014**, 35, 499–514.
- [3] X. Yang, C. Cheng, Y. Wang, L. Qiu, D. Li, *Science* **2013**, 341, 534–537.
- [4] M. D. Levi, M. R. Lukatskaya, S. Sigalov, M. Beidaghi, N. Shpigel, L. Daikhin, D. Aurbach, M. W. Barsoum, Y. Gogotsi, *Adv. Energy Mater.* **2015**, 5, 1400815.
- [5] R. Hou, G. S. Gund, K. Qi, P. Nakhanivej, H. Liu, F. Li, B. Y. Xia, H. S. Park, *Energy Storage Mater.* **2019**, 19, 212–241.
- [6] Q. Mahmood, M. G. Kim, S. Yun, S. M. Bak, X. Q. Yang, H. S. Shin, W. S. Kim, P. V. Braun, H. S. Park, *Nano Lett.* **2015**, 15, 2269–2277.
- [7] Q. Mahmood, S. K. Park, K. D. Kwon, S. J. Chang, J. Y. Hong, G. Shen, Y. M. Jung, T. J. Park, S. W. Khang, W. S. Kim, J. Kong, H. S. Park, *Adv. Energy Mater.* **2016**, 6, 1501115.
- [8] P. Nakhanivej, X. Yu, S. K. Park, S. Kim, J. Y. Hong, H. J. Kim, W. Lee, J. Y. Hwang, J. E. Yang, C. Wolverton, J. Kong, M. Chhowalla, H. S. Park, *Nat. Mater.* **2019**, 18, 156–162.
- [9] X. Cong, C. Cheng, Y. Liao, Y. Ye, C. Dong, H. Sun, X. Ji, W. Zhang, P. Fang, L. Miao, *J. Phys. Chem. C* **2015**, 119, 20864.
- [10] S. K. Park, P. Nakhanivej, H. S. Park, J. Korean, *Chem. Eng.* **2019**, 36, 1557–1564.
- [11] A. M. Navarro-Suárez, K. Maleski, T. Makaryan, J. Yan, B. Anasori, Y. Gogotsi, *Batteries & Supercaps* **2018**, 1, 33–38.
- [12] X. Yu, S. Yun, J. S. Yeon, P. Bhattacharya, L. Wang, S. W. Lee, X. Hu, H. S. Park, *Adv. Energy Mater.* **2018**, 8, 1702930.
- [13] L. Dong, W. Yang, W. Yang, Y. Li, W. Wu, G. Wang, J. Mater., *Chem. A* **2019**, 7, 13810–13832.
- [14] V. Augustyn, Y. Gogotsi, *Joule* **2017**, 1, 443–452.
- [15] M. Kota, H. S. Park, *Ceram. Int.* **2018**, 44, 3195–3200.
- [16] E. Pomerantseva, Y. Gogotsi, *Nat. Energy* **2017**, 2, 17089.
- [17] P. Simon, *ACS Nano* **2017**, 11, 2393–2396.
- [18] Y. Wen, K. He, Y. Zhu, F. Han, Y. Xu, I. Matsuda, Y. Ishii, J. Cumings, C. Wang, *Nat. Commun.* **2014**, 5, 4033.
- [19] C. Zhang, B. Anasori, A. Seral-Ascaso, S. H. Park, N. McEvoy, A. Shmeliov, G. S. Duesberg, J. N. Coleman, Y. Gogotsi, V. Nicolosi, *Adv. Mater.* **2017**, 29, 1702678.
- [20] O. Mashtalir, M. Naguib, V. N. Mochalin, Y. Dall'Agnese, M. Heon, M. W. Barsoum, Y. Gogotsi, *Nat. Commun.* **2013**, 4, 1716.
- [21] B. Ahmed, D. H. Anjum, M. N. Hedhili, Y. Gogotsi, H. N. Alshareef, *Nanoscale* **2016**, 8, 7580–7587.
- [22] R. Li, L. Zhang, L. Shi, P. Wang, *ACS Nano* **2017**, 11, 3752–3759.
- [23] C. Liu, Q. Xu, Q. Zhang, Y. Zhu, M. Ji, Z. Tong, W. Hou, Y. Zhang, J. Xu, J. Mater. Sci. **2019**, 54, 2458–2471.
- [24] M. Alhabeb, K. Maleski, B. Anasori, P. Lelyukh, L. Clark, S. Sin, Y. Gogotsi, *Chem. Mater.* **2017**, 29, 7633–7644.
- [25] J. Come, J. M. Black, M. R. Lukatskaya, M. Naguib, M. Beidaghi, A. J. Rondinone, S. V. Kalinin, D. J. Wesolowski, Y. Gogotsi, N. Balke, *Nano Energy* **2015**, 17, 27–35.
- [26] M. Q. Zhao, C. E. Ren, Z. Ling, M. R. Lukatskaya, C. Zhang, K. L. Van Aken, M. W. Barsoum, Y. Gogotsi, *Adv. Mater.* **2015**, 27, 339–345.
- [27] Q. Yang, Z. Huang, X. Li, Z. Liu, H. Li, G. Liang, D. Wang, Q. Huang, S. Zhang, S. Chen, C. Zhi, *ACS Nano* **2019**, 13, 8275–8283.

Manuscript received: November 20, 2019

Revised manuscript received: December 23, 2019

Accepted manuscript online: December 28, 2019

Version of record online: February 11, 2020